

Publications

---

6-20-2022

## Preliminary Study of Shape-Memory Alloy Torsional Tubes as Thermal Management Actuators Under Non-ideal Conditions

Paula Sanjuan Espejo  
*Embry-Riddle Aeronautical University, sanjuanp@my.erau.edu*

Samuel Desloover  
*Embry-Riddle Aeronautical University, desloovs@my.erau.edu*

Devon Hardy  
*Embry-Riddle Aeronautical University, hardyd6@my.erau.edu*

Mark Ricklick  
*Embry-Riddle Aeronautical University, ridlickm@erau.edu*

Frederick Calkin  
*The Boeing Company*

*See next page for additional authors*

Follow this and additional works at: <https://commons.erau.edu/publication>



Part of the [Aerospace Engineering Commons](#), and the [Heat Transfer, Combustion Commons](#)

---

### Scholarly Commons Citation

Espejo, P. S., Desloover, S., Hardy, D., Ricklick, M., Calkin, F., & Foutch, D. (2022). Preliminary Study of Shape-Memory Alloy Torsional Tubes as Thermal Management Actuators Under Non-ideal Conditions. *AIAA AVIATION 2022 Forum*, (). <https://doi.org/10.2514/6.2022-3372>

This Article is brought to you for free and open access by Scholarly Commons. It has been accepted for inclusion in Publications by an authorized administrator of Scholarly Commons. For more information, please contact [commons@erau.edu](mailto:commons@erau.edu).

---

**Authors**

Paula Sanjuan Espejo, Samuel Desloover, Devon Hardy, Mark Ricklick, Frederick Calkin, and David Foutch



# Preliminary Study of Shape-Memory Alloy Torsional Tubes as Thermal Management Actuators under Non-Ideal Conditions

Paula Sanjuan Espejo<sup>1</sup>, Samuel Desloover<sup>2</sup>, Devon Hardy<sup>3</sup>,  
and Mark Ricklick<sup>4</sup>

*Embry-Riddle Aeronautical University, Daytona Beach, FL, 32114, USA*

Frederick Calkins<sup>5</sup> and David Foutch<sup>6</sup>

*The Boeing Company, Seattle, WA 98124*

Shape-memory alloys (SMAs) have been used in many engineering applications because of their shape-memory effect and pseudoelasticity. SMA behavior is well understood under steady and constant temperature and loading conditions, whereas transient and non-ideal conditions effects should be further investigated. In this research, SMA torque tubes are studied for use in thermal management applications as self-regulated actuators responding to a process fluid with changes in temperature, with the goal of improved system efficiency by keeping components at an optimal temperature. When utilized in a thermal management configuration, it is likely that the SMA's thermal environment will be different than that to which it was trained for, leading to challenges from a modeling standpoint. Process fluid transients lead to temperature fluctuations in the SMA, which may not be negligible in a self-regulated system. Similarly, without perfect insulation of the SMA, a temperature gradient (potentially both along the length and along the thickness) will occur when the SMA is subject to a different boundary condition than what they were trained for (steady isothermal). Empirical efforts have shown that this leads to deviations from expected behavior, challenging the modeling of an open-loop system. This study looks at Nitinol (Nickel-Titanium alloy) rotational actuator tubes, with the goal further understanding the non-ideal conditions for a future model system. The SMA tube was subjected to both insulated and natural convection boundary conditions, with low and high mass flow rates for both heating and cooling cases. The one-dimensional model was compared to experiments as well as a modified thermal model to help improve modeling efforts. Experimental efforts show that a convection boundary leads to temperature gradients, especially at high temperatures and low flow rates. Thermal modeling showed no significant variation along the thickness, mostly due to the small thickness of the tube.

---

<sup>1</sup> PhD Student, Aerospace Engineering Department, Embry-Riddle Aeronautical University.

<sup>2</sup> Undergraduate Student, Aerospace Engineering Department, Embry-Riddle Aeronautical University.

<sup>3</sup> PhD Student, Aerospace Engineering Department, Embry-Riddle Aeronautical University.

<sup>4</sup> Associate Professor, Aerospace Engineering Department, Embry-Riddle Aeronautical University.

<sup>5</sup> Associate Technical Fellow, Boeing Research & Technology.

<sup>6</sup> Technical Fellow, Boeing Commercial Airplanes.

## I. Nomenclature

$A$	=	Area [m <sup>2</sup> ]
$A_s$	=	Austenite Start Temperature [°C]
$A_f$	=	Austenite Finish Temperature [°C]
$a_A, a_M$	=	Material Constants [1/°C]
$C_p$	=	Specific Heat at Constant Pressure [J/kg-°C]
$g$	=	Acceleration of Gravity [m/s <sup>2</sup> ]
$Gr$	=	Grashof Number
$h$	=	Heat Transfer Coefficient [W/m <sup>2</sup> -K]
$ID$	=	Inner Diameter [m]
$k$	=	Thermal Conductivity [W/m-K]
$L$	=	Length [m]
$M_s$	=	Martensite Start Temperature [°C]
$M_f$	=	Martensite Finish Temperature [°C]
$\dot{m}$	=	Mass Flow Rate [kg/s]
$Nu$	=	Nusselt Number
$OD$	=	Outer Diameter [m]
$Pr$	=	Prandtl Number
$q$	=	Heat Load [W]
$Re$	=	Reynolds Number
$SMA$	=	Shape-Memory Alloy
$T$	=	Temperature [°C or K]
$U$	=	Overall Heat Transfer Coefficient [W/m <sup>2</sup> -K]
$V$	=	Voltage [V]
$\alpha$	=	Angle of Twist [deg]
$\gamma$	=	Strain [%]
$\xi$	=	Fraction Martensite
$\nu$	=	Kinematic Viscosity [m <sup>2</sup> /s]

## II. Introduction

As system efficiencies improve, there is a general increase in component energy density, making thermal management an important aspect of modern design. However, thermal management systems add complexity and additional energy demands on the system. Thermal management optimization, such as flow control, can improve the overall efficiency of the system by ensuring components remain within optimal temperature limits, while avoiding excess energy consumption. In this research, shape-memory alloys (SMA) are considered as novel tools for self-regulated control of thermal management systems. Shape-memory alloys are a type of smart material that exhibit a mechanical response to temperature and/or loading changes. One of the most commonly used SMAs is Nitinol, a nickel-titanium alloy (NiTi), which will be used for this analysis. SMAs have been employed in different forms, including but not limited to wires and springs. Depending on the application, certain shapes are more beneficial. The approach explored here is a torsional tube.

Smart materials have seen an increase in applications in recent years. Developments regarding SMA applications have been more prominent in the biomedical and civil fields. SMAs have characteristics that are beneficial for biological applications such as high corrosion resistance and smart response that can mimic human tissue [1]. Civil engineering applications have been focused on passive dampening for structural control [2]. The aerospace engineering field has also seen applications of SMAs due to their ability to simplify systems promoting lightweight and silent solutions for actuation and control. Some examples include the Smart Wing program, in which SMA wires were used to actuate control surfaces; the SAMPSON project, in which SMAs were used to design a variable shape inlet for the engine of an F-15 aircraft; and the variable geometry chevrons created by The Boeing Company [3]. Most recently, The Boeing Company used SMAs to passively actuate deployable vortex generators on aircraft wings [4].

A brief review of SMAs is offered next. Shape-memory alloys have two main composition phases: austenite and martensite. The austenite phase, which is stable at high temperatures with a body-centered cubic structure, and the martensite phase, stable at lower temperatures and with a parallelogram asymmetric structure [2]. This solid-to-solid state transformation drives the mechanical response of the material. The martensite phase has two different variants: twinned and de-twinned. This transformation is dictated by loading and unloading of the material. There are two main characteristics that drive SMA applications in the engineering field: the shape-memory effect and pseudoelasticity.

As indicated by its name, the shape-memory effect is the ability of the material to “remember” a pre-determined shape. Upon deformation, the material retains the deformed shape until heated, after which it recovers its original shape [1]. This can be further exploited through training of the material; in which case it is referred to as two-way shape-memory effect. In this case, the material is trained to remember a form when heated to fully austenite and a different form when cooled down to fully martensite.

Different SMA materials and different tubes can be trained to respond to changes in different temperature ranges. These ranges are also affected by the loading experienced by the material. The mechanical response of the material occurs during the phase change from martensite to austenite and vice versa. When the SMA is heated, it will start to twist when the austenite start temperature,  $A_s$ , is exceeded. Fig. 1 shows the typical idealized percentage martensite versus temperature curve obtained from a phenomenological model. The limit temperatures can be observed:  $A_s$ ,  $A_f$ ,  $M_s$  and  $M_f$ . These temperatures characterize the SMA behavior, since they indicate the temperatures of phase changing, and are affected by loading. For the torsional tubes, the initial condition, with no twist, would be at full martensite. The tube will rotate during the phase change to fully austenite, beyond  $A_f$ , where full twist would be achieved. It is important to note that the cooling path to return to the original shape is not the same but occurs at different temperatures, dictated by  $M_s$  and  $M_f$ . Also note that if the temperature of the material changes during a phase changing process, minor loops are created as seen in the dashed line in Fig. 1, further complicating the simplified analysis of the tube behavior. The transformation response speed of the tubes is also an important factor in many applications. Different models have been presented to examine the behavior of SMAs, which can be divided mainly into phenomenological and microscopic physical models [5]. Liang & Roger’s one-dimensional constitutive model, [5], is used in this paper to compare to the experimental behavior of the tubes. Since this model is simple, complete accuracy is not expected.

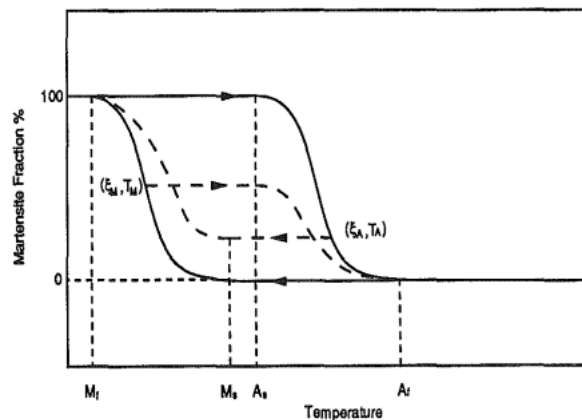


**Fig. 1 Martensite fraction versus temperature, cosine Liang-Rogers model [5].**

SMAs have both active and passive applications. Active applications involve an active control of the temperature and monitoring of the transformation, such as [6]. In passive applications the mechanical response is driven by a change in the temperature or loading conditions of the environment with no SMA response feedback, making the system self-regulated. For this paper, the focus will be in the shape change caused by the temperature effect in the material produced by the surrounding environment. A change in the temperature of the tubes leads to a torsional response which could be used as an actuator, such as a valve for flow control, which would be possible due to the high actuation strength of these materials. A change to the thermal conditions could present itself in ways such as a change in temperature of the process fluid in contact with the tube due to variations in system power levels. In this implementation, a fluid is passed through the tube, while one end of the tube remains fixed or clamped. If the flow is allowed to change temperature it will cause a mechanical response in the tube. The mechanical response will be the rotation of the free end of the tube. The amount of temperature change in the fluid determines the amount of twist that the tube will experience. As mentioned previously, the SMA tubes can be trained such that upon heating of the fluid, the free end of the tube is allowed to twist, and the original shape of the tube (zero twist) can be recovered by cool fluid. Such self-regulated or “passive” applications have seen limited implementation in the past; yet patents have been produced that include this approach: using SMAs actuators in charge of regulating the flowrate based on the temperature of the process fluid [7], and variable geometry heat-exchangers based on SMA actuation due to the temperature changes in the fluids [8,9]. Full understanding and modeling of the as-used behavior would enable improved use of these technologies.

The objective of this research is to utilize torsional SMA tubes as thermal management actuators due to their ability to produce large amount of torque and simplify actuator systems. Current applications focus mostly on full actuation of the SMA material. For thermal management systems, it is likely that the tubes are exposed to transient fluid behavior in terms of both temperature and loads, which makes the middle portion of the curve presented in Fig. 1 the main operation region. For this purpose, a better understanding of non-ideal conditions and the transition region of the SMA is required. The goal is to explore the behavior of the SMA tubes under controlled ideal and non-ideal thermal environments.

### III. Methodology

The proposed thermal management actuator consists of a process fluid flowing through an SMA tube as indicated in Fig. 2, which produces a twisting motion on the free end of the tube. Because of the finite rate of heat transferred from the fluid to the surrounding environment, there will be a fluid bulk temperature variation along the length of the tube. This will lead to potentially significant SMA temperature variations along the length of the tube. Similarly, due to the conduction through the tube, there is potential for temperature gradients between the inner and outer surfaces of the SMA. These effects must be considered as a real implementation would not likely operate under adiabatic or isothermal conditions. Knowledge of the temperature distribution is necessary to achieve predictable tube motion to allow fine actuation control.

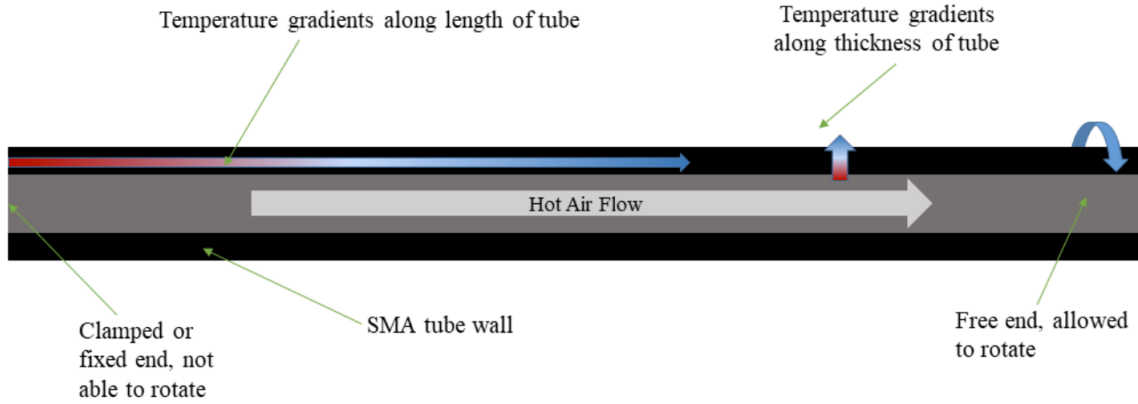


**Fig. 2 Schematic of SMA tube operation including temperature gradients.**

#### A. Thermal Modeling

Analytical calculations are produced to analyze the heat transfer through the torsional tube and the resulting system temperatures. Several assumptions are made to simplify this analysis: circumferentially averaged results, constant fluid properties for each segment, Reynolds number calculations based on constant conditions for each segment, and smooth surfaces. These calculations are used as a baseline comparison for the experimental results obtained. First, the heat transfer occurring radially is considered. The case of free convection on the outer surface of the tube is described here. Equations (1), (2), and (3) describe the heat transfer through convection from the process fluid to the tube, conduction through the wall, and free convection at the outer surface of the tube.

$$q_{conv,in} = h_{in}A_{in}(T_{bulk} - T_{wall,in}) \quad (1)$$

$$q_{cond} = \frac{2\pi k_{SMA}L_{SMA}(T_{wall,in} - T_{wall,out})}{\ln\left(\frac{OD}{ID}\right)} \quad (2)$$

$$q_{conv,out} = h_{out}A_{out}(T_{wall,out} - T_{ambient}) \quad (3)$$

Where  $h$  is the heat transfer coefficient,  $A$  is the appropriate surface area,  $T$  is the temperature,  $k$  is the thermal conductivity of the SMA tube,  $L$  is the length of the corresponding segment, and  $OD$  and  $ID$  are the outer and inner diameters of the tube.

The Nusselt number for convection inside the tube is calculated using the Dittus-Boelter correlation [10] shown in Eq. (4).

$$Nu_{in} = 0.023Re_{ID}^{0.8}Pr^{0.3} \quad (4)$$

Where  $Re$  is the Reynolds number, calculated using  $ID$  for the characteristic length, and  $Pr$  is the Prandtl number.

The Nusselt number for free convection over a horizontal cylinder is obtained using Churchill and Chu's correlation [10] shown in Eq. (5).

$$Nu_{out}^{\frac{1}{2}} = 0.6 + 0.387 \left\{ \frac{GrPr}{\left[ 1 + (0.559/Pr)^{\frac{9}{16}} \right]^{\frac{16}{9}}} \right\}^{1/6} \quad (5)$$

Where the Grashof number,  $Gr$ , is defined in Eq. (6).

$$Gr_{out} = \frac{g \left( \frac{1}{T_{ambient}} \right) (T_{wall,out} - T_{ambient}) OD^3}{\nu_{ambient}^2} \quad (6)$$

Where  $g$  is the acceleration due to gravity and  $\nu$  is the kinematic viscosity. Here,  $T_{ambient}$  is in Kelvin for the  $1/T_{ambient}$  component.

The heat transfer coefficient values are obtained from the definition of Nusselt number, and the properties of air are calculated based on ideal gas principles and Sutherland's laws at the appropriate temperature. Since  $q_{conv,in} = q_{cond} = q_{conv,out} = q_r$ , not considering other forms of heat leakage, the two unknowns in Eqns. (1-3) are the inner and outer temperature of the wall.  $q_r$  is the heat in the radial direction and is calculated using the overall heat transfer coefficient,  $U$ , as shown on Eqns. (7) and (8), and then used to determine the wall temperatures. Note since the outer wall temperature is a part of the Grashof number calculation; indirect solution methodology is required to obtain the desired temperature values.

$$UA = \frac{1}{\frac{1}{A_{in}h_{in}} + \frac{\ln \left( \frac{OD}{ID} \right)}{2\pi k_{SMA}L_{SMA}} + \frac{1}{A_{out}h_{out}}} \quad (7)$$

$$q_r = UA(T_{bulk} - T_{ambient}) \quad (8)$$

The torsional tube is then discretized lengthwise using energy balance marching technique of heat transfer along the tube, so that  $q = q(x)$ . To mimic the experiment, in which four thermocouples are placed on the outer surface of the tube, the SMA is divided into four segments. The tube is discretized in segments of length 28 mm, 23 mm, 22 mm, 14 mm, and 13 mm so that the locations of the thermocouples correspond with the outlet of a segment, starting from the outlet of the tube (placement of thermocouples is described later). The  $q_r$  calculated previously is also the heat lost by the process fluid in that tube segment,  $q(x) = q_r$ , so that the temperature "exiting" the given segment and therefore "entering" the next tube segment is calculated using Eqn. (9). Therefore, note that for the above equations, (1) to (8),  $T$  is  $T(x)$ ,  $h$  is  $h(x)$ ,  $A$  is  $A(x)$ , etc., corresponding to the appropriate segment along the tube.

$$q(x) = \dot{m}C_p(T_{bulk_{in}}(x) - T_{bulk_{out}}(x)) \quad (9)$$

Where  $\dot{m}$  is the mass flow of the process fluid and  $C_p$  the specific heat at constant pressure.

Through these calculations, the temperature gradients along the thickness and the length of the tube are estimated and used for reference and comparison to experimental results.

## B. SMA Response Modeling

Liang and Rogers [5] one-dimensional thermomechanical constitutive model for SMAs is compared to experimental results. The results presented in this paper are focused on no stress applied to the tube, and so the equations presented next for the Liang-Rogers model are only valid at no-stress conditions. This model utilizes cosine

functions to describe the phase changing process of the SMA material. The fraction martensite,  $\xi$ , equations for heating in Eq. (10) and cooling in Eq. (11) processes are shown below.

$$\xi = \frac{\xi_0}{2} \cos(a_A(T_{SMA} - A_s)) \quad (10)$$

$$\xi = \frac{1 - \xi_0}{2} \cos(a_M(T_{SMA} - M_f)) + \frac{1 + \xi_0}{2} \quad (11)$$

Where  $\xi_0$  is the initial fraction of martensite. This value is 1 when the process starts from a completely cooled SMA tube, with full martensite composition, but might vary for different tests if the initial point is a heated tube. If the process being considered starts halfway through the actuation, at a state with a mix of austenite and martensite, this value will be 0.5. This initial fraction of martensite value is important for the modeling of the minor loops.  $T_{SMA}$  is the temperature of tube, and  $A_s$  and  $M_f$  were defined previously as austenite start and martensite finish temperatures. The constants  $a_A$  and  $a_M$  are obtained through Eqns. (12) and (13).

$$a_A = \frac{\pi}{A_f - A_s} \quad (12)$$

$$a_M = \frac{\pi}{M_s - M_f} \quad (13)$$

Note that the Liang-Rogers model only considers SMA materials for which  $A_s \geq M_s$  [5].

It is assumed that there is a direct correlation between the martensite fraction and the actuation of the tube. Therefore, for  $\xi=0$ , at full austenite, the tube is fully actuated at its maximum strain value,  $\gamma_{max}$ , and maximum angle of twist,  $\alpha_{max}$ . For modeling purposes, the current strain value is calculated based on Eq. (14).

$$\gamma = \gamma_{max}(1 - \xi) \quad (14)$$

The relationship between the angle of twist and the strain is described by Eq. (15), where  $\alpha$  is in degrees and  $\gamma$  in percentage form.

$$\alpha = \frac{2L_{twist}(\gamma/100)}{OD} \frac{180}{\pi} \quad (15)$$

Note that  $L_{twist}$  is not the full length,  $L_{SMA}$ , of the torsional tube.  $L_{twist}$  is the length of the tube that will twist, excluding the splined ends.

### C. Shape-Memory Alloy Torsional Tube Characteristics

The Nickel-Titanium (NiTi) alloy tube used for this analysis has an outer diameter of 9.6 mm and inner diameter of 7.5 mm. The length of the tube is 100 mm, with splined ends on both sides that are used to properly support the tube within the setup, which are 6 mm in length. Therefore, the active length of the tube is 88 mm. An image of the tube is included in Fig. 3.

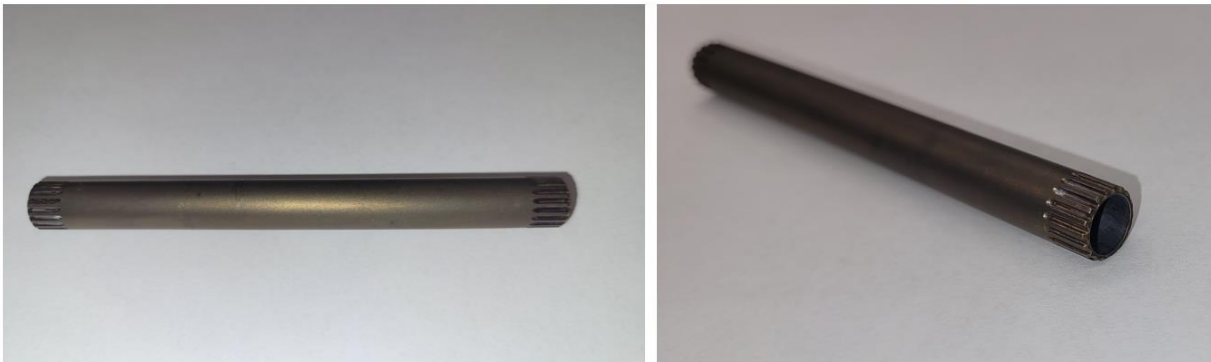


**Fig. 3. Views of NiTi SMA tube.**

This tube has been trained to produce a two-way shape-memory effect. Following characterization training data of the tube, the maximum strain for this tube is 3.9%, which yields a maximum twist angle of  $41^\circ$ , calculated analytically through Eq. (15). During a heating experiment, in which the temperature of the SMA is increasing, the twisting of the tube is expected to start occurring at the austenite start temperature,  $A_s$ ,  $60.3^\circ\text{C}$ . Maximum twist is expected at the austenite finish temperature,  $A_f$ , which is  $78.7^\circ\text{C}$ . When the tube is at a temperature equal or higher than this, and the heat input is stopped so that the tube starts cooling, twisting in the opposite direction starts at the martensite start temperature,  $M_s$ ,  $64.4^\circ\text{C}$  and fully recovers its initial, untwisted state at the martensite finish temperature,  $M_f$ ,  $38.9^\circ\text{C}$ . These temperatures were obtained from training data and not experimentally in this research.

#### D. Experimental Setup

An experimental facility, for which the schematic is described in Fig. 4 was developed to study the response of the SMA torque tube to different thermal conditions. Heated air, which is the chosen process fluid for the current study, flows through the torsional SMA tube and the mechanical and thermal response of the tube is recorded for comparison with analytical and model results. The setup, a schematic included in Fig. 4, was designed to allow different fluid temperature and flow rate settings under various external thermal conditions (e.g. insulated or uninsulated).

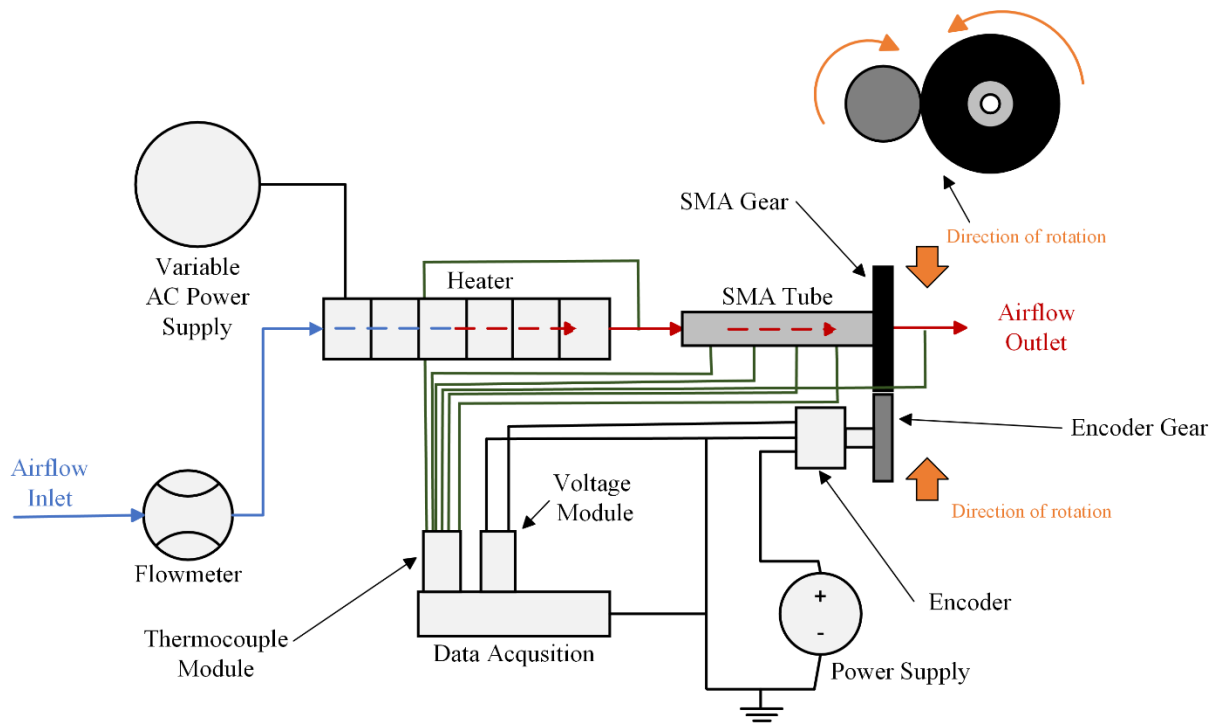


**Fig. 4 Experimental setup schematic.**

To achieve this, a torque tube is suspended at one end and connected to a heated air supply at the other. The suspended end is free to rotate, and the degree of rotation is measured. The experimental setup consists of an open flow loop supplied with compressed shop air and exiting to the atmosphere after travelling through a heater followed by the SMA tube. At the beginning of the setup, air runs through a Brooks Instrument flowmeter, measuring 1-8 SCFM (standard cubic feet per minute) with a minimum full-scale accuracy of 5%. The flow is heated before travelling to the SMA, using an OMEGA inline duct heater with a maximum power of 200 W at 120 VAC. The heater is supported on both ends using 1" ID T-Slotted framing mounting brackets. It is powered by a VARIAC (3PN2210B-DAM) variable voltage supply.

SMA inlet air temperatures are measured after the heater at a T-fitting with two type-T thermocouples ( $\pm 1^\circ\text{C}$ ). The flow then transitions to the clamped portion of the SMA via a low conductivity, high temperature tubing. Before entering the SMA torque tube, the air travels through a short section of 1/4" NPT threaded pipe on one end. The end of this pipe section fits with the SMA hex adapter. The hex adapter is clamped between two custom Delrin blocks (3.25" long, 3/4" wide, and 1/2" tall), and adapts the splined end of the SMA to the air supply. The Delrin blocks are secured to the support rail using a channel nut with the threaded rods which is modular for different length SMA tubes.

Attached to the splined end of the hex adapter as a cantilever beam, the SMA hangs off the end of the T-slotted aluminum frame. To measure the rotation of the SMA, an ERCF 2410 Z 90 encoder is utilized. The encoder is connected to the SMA through a 2.08 gear reduction, with a 75 tooth, 75 mm pitch diameter gear connected to the SMA and a 36 tooth, 36 mm pitch diameter gear attached to the encoder. It was ensured that the smaller gear was attached such that the encoder starts at a recorded low value of twist and is still in full tooth engagement with the larger gear. Gears allows for improved resolution of the rotation. The resolution of the encoder in this setup is 12 bits over 43.3 degrees of rotation of the SMA, corresponding to a voltage signal range of 0 to 10 V over the same range. An OMEGA PST 4130 power supply is used to power the encoder at 15 VDC.

Temperature along the SMA is measured using type-T thermocouples made in house. The thermocouple bead is mounted to touch the SMA using hose clamps to ensure contact. Eight thermocouples, two at each of the following locations, starting from the outlet: 28 mm, 51 mm, 73 mm, and 87 mm. Note the gear mounted at the outlet of the thermocouple is 20 mm thick and it is not easy to place the thermocouples at an exact equidistant distance. The flow temperature at the air outlet is measured using two thermocouples attached to the SMA gear and in direct contact with the airflow. To simulate adiabatic conditions, fiberglass insulation was placed around the SMA and connections to minimize heat leakage. The thermocouples along the length of the tube are labeled as TC 1, TC 2, TC 3, and TC 4 starting from closest to the process fluid inlet.

The data acquisition device used in this setup is a National Instruments NI cDAQ-9174. A NI 9213 24 bit module is used to record the data from the six thermocouples and a NI 9205 16 bit module connected to a DB37-M2 plug breakout terminal is used to record the voltage output from the encoder. The data is then recorded and processed using a MATLAB code. Data is recorded at the rate of 10 samples per second.

The range for the encoder is 0° to 90° with an output voltage of 0 to 10 V, with +/- 0.5% linearity. Therefore, the angle recorded in MATLAB is just 9 times the voltage output,  $V$ , of the encoder. The gear reduction ratio used is 2.08. Therefore, the angle of twist of the SMA tube in degrees,  $\alpha$ , based on the output voltage of the encoder for this application follows the formula on Eqn. (16).

$$\alpha = V * 9 * \frac{1}{2.08} \quad (16)$$

The data presented in this paper includes temperature of all thermocouples, including the air inlet and outlet, versus time, and angle of twist of the SMA tube versus time.

## E. Test Matrix

The test matrix utilized in this study is shown below. The goal is to observe variation between insulated (isothermal) and non-insulated (natural convection boundary) cases, at a high and a low flow rates. For isothermal tests, the tube is wrapped in insulation to provide an environment as close to the tube's training as possible. For convection cases, the insulation around the tube is removed. For all tests shown below, the power setting is increased to the desired value and the system is left to reach steady-state. The two cooling cases are continuations of the previous test. The purpose of Test 2 is repeatability. Tests 1, 2, 7 are also used as transient examples to analyze the twist of the tube over the maximum range of temperature allowed by the setup, hence the lower flow rate for the initial tests. For these tests, data of the tube heating up from room temperature to steady-state and cooling back down is analyzed.

1. Isothermal Boundary Condition (Insulated)
  - a. Test 1 – Maximum strain testing, 157 W, 0.000547 kg/s
  - b. Test 2 – Repeatability of Test 1, 157 W, 0.000547 kg/s
  - c. Test 3 – Heating, 164 W, 0.0011 kg/s
  - d. Test 4 – Cooling, 118 W, 0.0011 kg/s (continuation from Test 3)
  - e. Test 5 – Heating, 144 W, 0.0011 kg/s
  - f. Test 6 – Heating, 119 W, 0.000547 kg/s
2. Natural Convection Boundary Condition
  - a. Test 7 – Maximum strain testing, 157 W, 0.000547 kg/s
  - b. Test 8 – Heating, 164 W, 0.0011 kg/s
  - c. Test 9 – Cooling, 118 W, 0.0011 kg/s (continuation from Test 6)
  - d. Test 10 – Heating, 119 W, 0.000547 kg/s

## IV. Results

In the results provided below, one of the thermocouples at TC 4 was discarded for faulty readings. For flow temperature measurements at the outlet of the heater and the outlet of the tube, the highest value of the two thermocouples at each location is presented here. For Tests 1, 2, and 7 the angle of twist is plotted versus the average temperature of the tube at inlet at TC 2 in Fig. 5. Minor heat leakage is observed in TC 1 in some of the tests due most likely to connections, so the maximum temperature in the tube is presented in the data below at TC 2, which is also near the inlet. These tests are carried out at low flow rate and high power setting, with Test 7 being non-insulated. Even though Tests 1 and 2 have the same settings and are both insulated cases, some variation is seen in the maximum strain and temperature reached by the tube, from 2.88% to 2.73%, and 112.8°C to 105.9°C. This is likely due to instrumentation error, since the flow meter has a visual reading and manual adjustment, and the power setting is also manual and with some error. For isothermal cases “Tube Temperature” is calculated as the average along the tube, while for convection cases is refers to TC 2 data exclusively.

Most of the SMA twisting capabilities occur between  $A_s$ - $A_f$  during heating and  $M_s$ - $M_f$  in cooling. From Fig. 5, it can be seen that in the right side of the curve, heating, most of the twist occurs between 60.3°C and 78.7°C. Therefore, a small change in temperature in this region leads to a significant angle of twist range. After 78.7°C, the angle of twist change with temperature of the tube has a considerably lower slope. Therefore, the fact that there is no considerable difference between the angle shown in Table 1 for the different tube temperature conditions is not surprising, even though there is a convection condition in Test 7. The rest of the testing cases are focused on the region of the curve with the maximum twist per degree Celsius. Fig. 5 also helps appreciate the different heating and cooling paths. For instance, an angle of 15° could be achieved at a temperature of 71°C during heating and a temperature of 56°C during cooling. From the data in Table 1 it is concluded that the maximum twist observed is 30.4°, therefore the maximum strain observed is 2.88%, at a maximum tube temperature of 112.8°C.

**Table 1. Summary of initial testing.**

	Angle of Twist	Tube Temperature	Heater Exit Flow Temperature	Tube Outlet Flow Temperature	Ambient Temperature
Test 1	30.4°	112.8°C	144.1°C	112.7°C	-
Test 2	28.9°	105.9°C	132.2°C	103.7°C	-
Test 7	27.9°	99.1°C	139.5°C	105.8°C	21.4°C

Differences are recorded between characterization data and experiments in terms of strain, 3.9% for characterization data and 2.88% for experimental data. The strain is calculated from the angle of twist using Eqn. (15). The current setup does not allow as high temperatures in the tube as those seen in training data, so that also affects the different strain values. For modeling purposes and comparison to the Liang-Rogers model, the experimental maximum strain is used. This comparison is shown in Fig. 6, in which the temperature input to the model is that from Test 1, TC 2. Remember that the Liang-Rogers model assumes that the SMA under consideration follows the relation  $A_s \leq M_s$ , which does not hold for the current tube. Since  $A_s$  and  $M_s$  are close, an adjusted model is considered in which  $A_s \geq M_s$ , which is also included in Fig. 6. The temperatures are adjusted so that  $A_s$  is 64°C,  $M_s$  is 63°C, and  $A_f$  is increased by 10°C to better match the experimental data. These adjustments are done to be able to use the model as a comparison, therefore matching of the experimental data is not expected, especially based on the wider curve produced by the adjusted model. This comparison to a simple model is still valuable to further develop the modeling approach based on the results. Fig. 7 and Fig. 8 show the recorded temperatures for Test 1 and for Test 7 as examples of data collection and to show the temperature change over time.

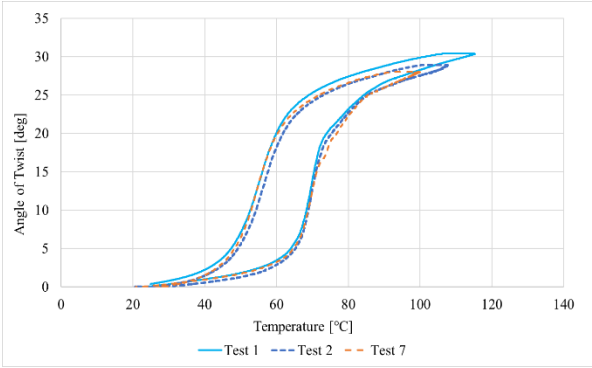


**Fig. 5** Angle of twist versus tube temperature, transient effects.

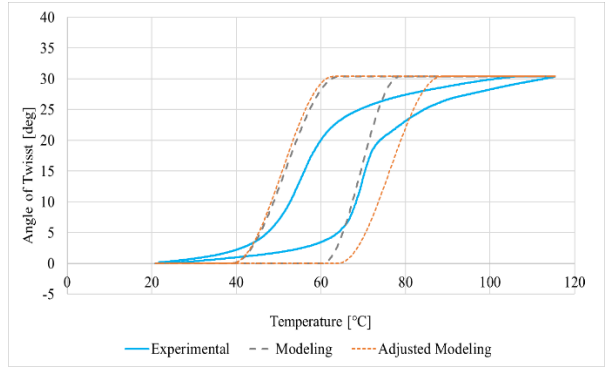


**Fig. 6** Comparison of experimental data to Liang-Rogers model and adjusted model.

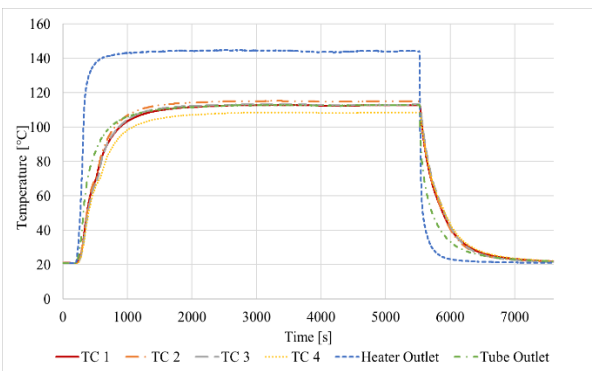


**Fig. 7** Temperatures versus time for Test 1.

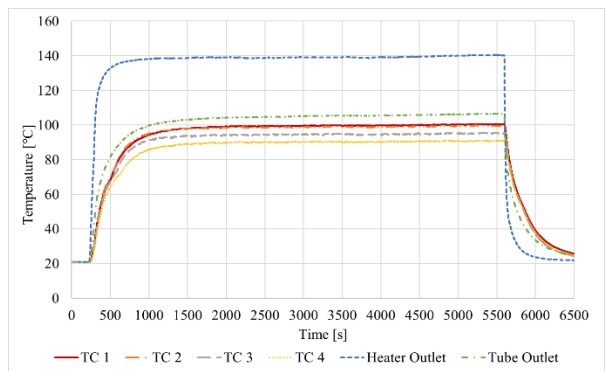


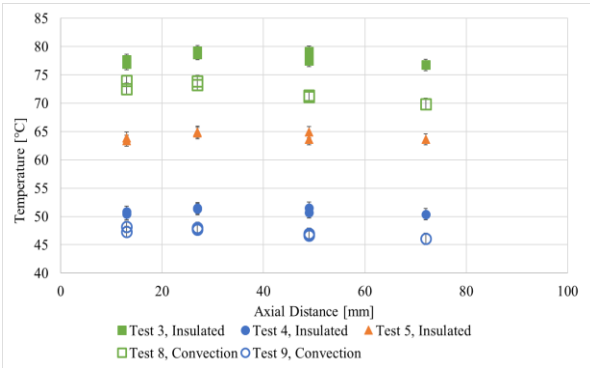
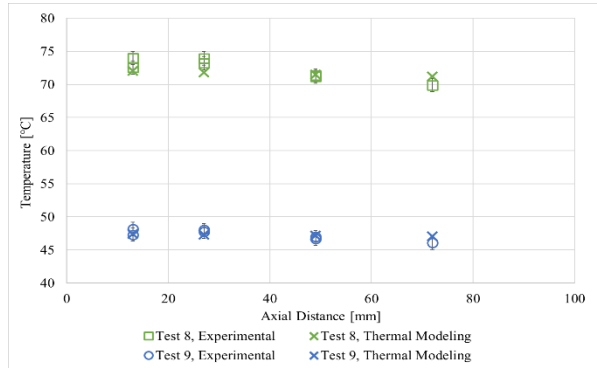
**Fig. 8** Temperatures versus time for Test 7.

Tests 3 through 5 are isothermal tests (insulated, high flowrate). Fig. 9 shows the temperature variation recorded at steady-state along the tube (axial temperature), where 0 mm indicates the flow inlet of the tube. Steady-state is considered when changes  $<1^{\circ}\text{C}$  over a span of 25 minutes are observed. The data from all isothermal tests show good agreement with the expected results. The error bars in these plots show the error due to type-T thermocouple measurements,  $\pm 1^{\circ}\text{C}$ . Tests 8 and 9 are convection cases imitating the flow and power settings of Tests 3 and 4. The variation of temperature along the tube is also included in Fig. 9. It is likely that in a thermal management implementation, full insulation of the tubes is not possible and therefore heat loss (and a corresponding gradient along the length of the tube), in this case in the form of free convection, should be examined. The temperature of the process fluid exiting the heater is recorded and for both sets of tests is comparable, therefore the power setting similarity is confirmed.

Table 2 includes relevant values obtained in these tests. There is considerable heat lost between the heater flow exit and the tube despite the insulation placed that will be improved in the future. There is an important effect of heating versus cooling, which can be seen between Tests 4 and 5. For Test 5, a higher average tube temperature provides a lower angle of twist than that obtained in Test 4, which has a lower average tube temperature. The convection cases show a decrease of tube temperature along the tube, especially evident in Test 8 with a  $4^{\circ}\text{C}$  drop. The thermal modeling and experimental cases are compared in Fig. 10. The thermal model seems to underestimate the values towards the inlet of the tube. This might be an effect caused by other forms of heat loss. This data also shows the effects of the convection boundary are larger at higher tube temperatures. Radial variation calculations for the inner surface temperature of the tube were carried out, but due to the small thickness of the tube under consideration, these variations are not significant. Table 2 includes a summary of the high flow rate cases. It can be seen that there is a difference between the isothermal and convection cases in terms of SMA tube response. Tests 3 and 8 have a large difference in angle of twist,  $5^{\circ}$ . The modeling predicted angle is not accurate and for most cases, falls within the range created by the non-adjusted and adjusted models.

**Table 2. High flow rate test results summary.**

	Angle of Twist	Tube Temperature	Heater Exit Flow Temperature	Tube Outlet Flow Temperature	Ambient Temperature	Model Predicted Angle [Not Adj./Adjusted]
Test 3	21.3°	78.0°C	88.6°C	75.7°C	-	30.3°/18.4°
Test 8	16.4°	73.6°C	90.6°C	76.2°C	21.3°C	25.0°/10.0°
Test 4	7.6°	51.0°C	56.4°C	50.0°C	-	13.9°/9.2°
Test 9	4.9°	47.9°C	56.2°C	49.3°C	21.4°C	6.9°/3.1°
Test 5	3.1°	64.1°C	72.1°C	63.2°C	-	3.1°/0.001°

**Fig. 9 High flow rate testing, surface temperature along tube.****Fig. 10 Thermal modeling for Tests 8 and 9.**

The low flow tests are presented next. Tests 1 and 6 are insulated while 7 and 10 are not. Similar data to that presented for the high flow rate cases is included in Fig. 11 and Fig. 12. Table 3 includes the summary of the tests for low flow rate testing. Note that Test 7, at low flow rate and high power setting, has the largest temperature drop along the tube from all tests considered, around 10°C. However, it does not present the largest angle of twist difference since the temperature of the tube is past  $A_f$ . In the transient portion of Test 7, difference can be seen along the thermocouples in Fig. 13, which includes TC 2, TC 3, TC 4, and an average of the temperatures along the tube. For an angle of twist of 15°, TC 2 is at 71°C, TC 3 is at 69°C, and TC 4 is as 66°C. Since these values lie between  $A_s$  and  $A_f$ , a model would produce significantly different angle of twist predictions depending on the temperature chosen. Tests 6 and 10 have the largest angle of twist difference, 7.6°, of all the tests. Low flow rate cases see an increased effect of temperature gradients.

**Table 3. Low flow rate results summary.**

	Angle of Twist	Tube Temperature	Heater Exit Flow Temperature	Tube Outlet Flow Temperature	Ambient Temperature	Model Predicted Angle [Not Adj./Adjusted]
Test 1	30.4°	112.8°C	144.1°C	112.7°C	-	30.4°/30.4°
Test 7	27.9°	99.1°C	139.5°C	105.8°C	21.4°C	30.4°/30.4°
Test 6	11.9°	72.0°C	86.8°C	70.6°C	-	21.5°/7.1°
Test 10	4.2°	66.6°C	86.8°C	69.6°C	21.6°C	8.0°/0.8°

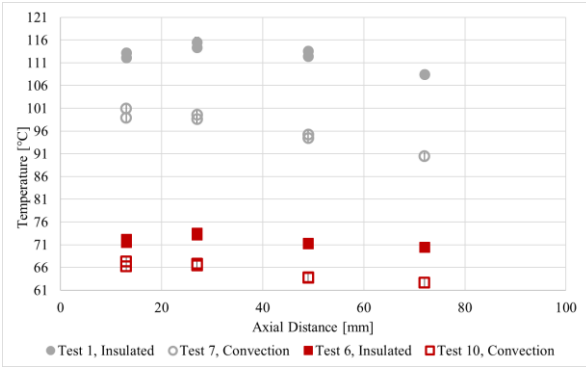


**Fig. 11** Low flow rate testing, surface temperature along tube.

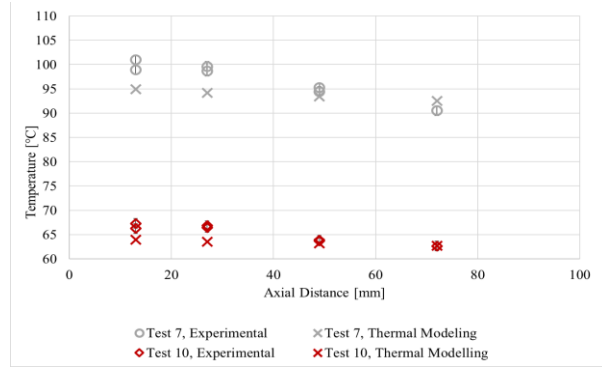


**Fig. 12** Thermal modeling for Tests 7 and 10.

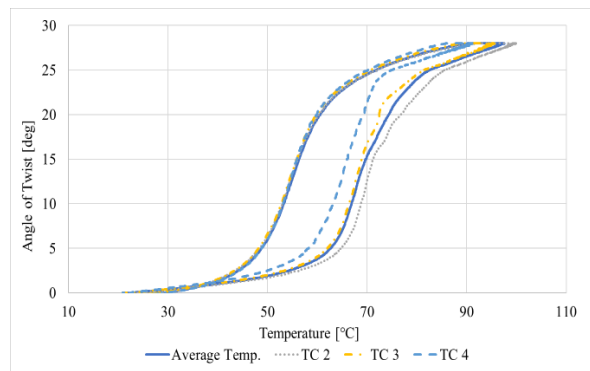


**Fig. 13** Comparison between thermocouples for Test 7.

Fig. 14 includes a summary of all the steady-state angles of twist for each case. The variation between the cases at Test 1 is probably due to the temperature used for plotting. Remember that for isothermal cases the tube temperature is taken as the average while for convection cases the tube temperature is taken as the maximum tube temperature, TC 2.

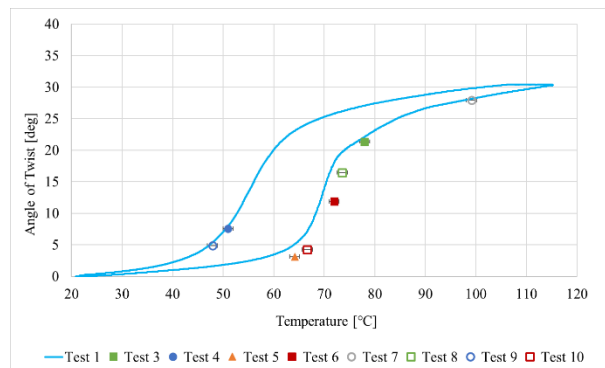


**Fig. 14** Steady-state angle of twist for each case superposed over Test 1.

## V. Conclusion and future work

In this research, a two-way shape-memory SMA torsional actuator was used to better understand the behavior of SMAs under non-ideal conditions for thermal management systems implementation. Experimental tests were carried out and compared with the one-dimensional Liang-Rogers model and a thermal analytical model. The test matrix consisted of 10 tests with varying inlet temperature and mass flow of the air entering the SMA tube, as well as two boundary conditions for the exterior surface of the SMA: insulated and natural convection.

Looking at how the isothermal and natural convection boundary conditions compared, variation in the angle of rotation obtained by the SMA was observed. This difference is most notable between 60.3°C and 78.8°C when heating, in the transformation region from martensite to austenite. When comparing the twist rate for similar inlet temperatures, with an inlet temperature of approximately 89°C, the SMA rotated 4.9° more when the SMA was insulated compared to when the tube was not insulated. During the low flow rate tests with a similar power setting of the heater, similar results were shown. These experiments showed a 7.4°C difference of the SMA rotation; allowing the tube to rotate to 11.8° when insulated and only 4.2° when subjected to the natural convection boundary condition. The experiments also looked at examining maximum strain for the SMA tubes at the current testing rig settings, which resulted in a rotation of 30.4° and a maximum strain of 2.88% when the SMA tube is at a temperature of 112.8°C. Low flow rate and high power setting tests have the largest temperature gradient along the length of the tube, around 10°C. At higher flow rate, the largest gradient was about 4°C. Additionally, in the transient portion of the high flow rate high power setting test, differences can be seen along the thermocouples, for an angle of twist of 15°, TC 2 is at 71°C, TC 3 is at 69°C, and TC 4 is at 66°C. Since these values lie between  $A_s$  and  $A_f$ , a model would produce significantly different angle of twist predictions depending on the temperature chosen.

There were some discrepancies between the experiments and the SMA model. This was expected as the model is one-dimensional while the experimental rotational motion is more complex. The thermal model shows general good agreement but underestimates the temperature gradient in the tube towards the inlet. In future work, to better improve the modeling of the system, improvements on the current model, or a combination of different SMA models would need to be used to better represent the non-ideal conditions and torsional tube behavior. For the tubes tested, radial temperature variations were considered but inner wall temperatures were not reported because the calculations lied within 0.5°C of the outer wall temperature, most likely due to the small thickness of the tubes.

The next efforts would concentrate on continuing testing, especially exploring transient effects and “inner loops”. With more experimental cases, more data will help refine the model and help determine which models to use and how to obtain a better representation of the system. Future efforts will also include Computational Fluid Dynamics (CFD) cases. The experimental data will then be compared to the CFD results to improve modeling efforts of the system.

## References

- [1] Jani, J. M., Leary, M., Subic, A., and Gibson, M. A., “A review of shape memory alloy research, applications and opportunities,” *Materials and Design*, Vol. 56, 2014, pp. 1078- 1113.  
doi: 10.1016/j.matdes.2013.11.084
- [2] Song, G., Ma, N., and Li, H.-N., “Applications of shape memory alloys in civil structures,” *Engineering Structures*, Vol. 28, No. 9, 2006, pp. 1266-1274.  
doi: 10.1016/j.engstruct.2005.12.010
- [3] Hartl, D. J., and Lagoudas, D. C., “Aerospace applications of shape memory alloys,” *Proceedings of the Institution of Mechanical Engineers. Part G, Journal of Aerospace Engineering*, Vol. 221, No. 4, 2007, pp. 535-552.  
doi: 10.1243/09544100JAERO211
- [4] Calkins, F.T., Fassmann, A.W., Vijgen, P.M., Nicholson, D.E., Bass, M.A., Benafan, O., Gaydosh, D.J., Bigelow, G.S., and Noebe, R.D., “SHAPE MEMORY ALLOY ACTUATED VORTEX GENERATORS: Shape memory alloy reconfigurable technology-vortex generators (SMART-VG) can reduce fuel consumption and improve aircraft efficiency,” *Advanced Materials & Processes*, Vol. 178, No. 3, 2020, pp. 60-63.
- [5] Liang, C., and Rogers, C. A., “One-dimensional thermomechanical constitutive relations for shape memory materials,” *Journal of Intelligent Material Systems and Structures*, Vol. 8, No. 4, 1990, pp. 285-302.  
doi: 10.1177/1045389X9700800402
- [6] Zhakipov, Z., Huang, J., and Paik, J., “A Novel Torsional Shape Memory Alloy Actuator: Modeling, Characterization, and Control,” *IEEE Robotics & Automation Magazine*, Vol. 23, No.3, 2016, pp. 65-74.  
doi:10.1109/MRA.2016.2582868
- [7] Foutch, D. W., and Calkins, F. T., The Boeing Company, Chicago, IL, U.S Patent for a “thermal management system incorporating shape memory alloy actuators and related methods,” No. US 10,612,867 B2, filed 11 Apr. 2020.
- [8] Diaz, C. E., Gerstler, W. D., Storage, M. R., and Kenworthy, M. T., General Electric Company, Niskayuna, NY, U.S Patent for a “variable geometry heat exchanger apparatus,” No. US 9,903,274 B2, filed 27 Feb. 2018
- [9] Raimarckers, N., Borbouse, C., Cornet, A., and Bajusz, D., Techspace Aero S.A., Milmort, BE, U.S Patent for “integration of a surface heat-exchanger with regulated air flow in an airplane engine,” No. US 2021/0168115 A1, filed 5 Jul. 2012
- [10] Holman, J. P., *Heat Transfer*, 10<sup>th</sup> ed., McGraw Hill Higher Education, New York, 2010, Chaps. 6, 7.